Journal of Laser Applications

Fabrication of Pd/WO_3 colloidal nanoparticles by laser ablation in liquid of tungsten for optical hydrogen detection

Cite as: J. Laser Appl. **31**, 032018 (2019); https://doi.org/10.2351/1.5110352
Submitted: 16 May 2019 . Accepted: 02 August 2019 . Published Online: 22 August 2019

H. Kalhori, M. Ranjbar, H. Farrokhpour, and H. Salamati

View Online Export Citation CrossMark

ALIA
AIP Publishing

© 2019 Author(s).

Journal of Laser Applications | ARTICLE | scitation.org/journal/jla

Fabrication of Pd/WO_3 colloidal nanoparticles by laser ablation in liquid of tungsten for optical hydrogen detection

Cite as: J. Laser Appl. **31**, 032018 (2019); doi: 10.2351/1.5110352
Submitted: 16 May 2019 · Accepted: 2 August 2019 ·
Published Online: 22 August 2019

View Online Export Citation CrossMark

H. Kalhori,[1] M. Ranjbar,[1,a)] H. Farrokhpour,[2] and H. Salamati[1]

AFFILIATIONS

[1]Department of Physics, Isfahan University of Technology, Isfahan 84156-8311, Iran
[2]Department of Chemistry, Isfahan University of Technology, Isfahan 84156-8311, Iran

[a)]**Author to whom correspondence should be addressed; electronic mail:** ranjbar@cc.iut.ac.ir

ABSTRACT

In this paper, tetragonal WO_3 colloidal nanoparticles (NPs) were prepared by pulsed laser ablation in liquid of tungsten target in de-ionized water, followed by adding a $PdCl_2$ solution immediately after the ablation process or hours after aging. X-ray photoelectron spectroscopy revealed that the surface chemical composition is a mixture of W^{5+}, W^{6+}, and O–H groups for which a defective $WO_{2.8}$ surface composition was calculated. Transmission electron microscope images showed that only when $PdCl_2$ is added immediately, Pd/WO_3 core-shell NPs are formed spontaneously. UV-Vis spectrophotometry showed an increase in the optical bandgap due to NPs oxidation throughout the aging period. Thus, the spontaneous formation of the Pd/WO_3 core-shell NPs was attributed to the presence of surface oxygen defects in newly formed NPs. With hydrogen exposure (<10%), Pd/WO_3 solutions turned blue, indicating a gasochromic coloration ability which was used to detect different hydrogen concentrations below 10%. The dynamic response to different hydrogen concentrations was also studied at 630 nm constant wavelength. The results revealed that Pd/WO_3 NPs obtained by the pristine WO_3 colloidal solution show a better gasochromic performance, in both the coloration and response time.

Key words: laser ablation in liquid, WO_3 NPs, $PdCl_2$, aging, core-shell, gasochromic, hydrogen sensing

Published under license by Laser Institute of America. https://doi.org/10.2351/1.5110352

I. INTRODUCTION

WO_3 nanoparticles (NPs) have great potential to be used in the gas sensors, especially for hydrogen gas[1–3] As a well-known type of hydrogen sensing, in the gasochromic effect the optical properties of WO_3 change reversibly from a transparent to a blue state up on hydrogen[4–6] so that it can be used as a visual hydrogen sensor material.[7] In these gas detecting platforms, a thin catalytic layer of Pd or Pt deposited over the WO_3 NPs is required to enable hydrogen decomposing into H atoms and allows them to inject into the material lattice prior to the coloration. Therefore, many attempts on the gasochromic properties of materials focus on the catalyst and the active gasochromic material preparation. Although many sensors are working in gaseous media, detection of hydrogen in aqueous media like water can be important in environmental sciences, biomedical sciences, biotechnology, research on photochemical water splitting, and H_2 enriched drinking water. For example, drinking water enriched with dissolved hydrogen has been reported to have a positive effect on many health and well-being conditions. Therefore, water base liquid hydrogen detector, especially based on optical and vision methods, is of great importance. Now some discussion about the potential application of our samples is added to the Introduction section. Moreover, the colloidal solution of Pd/WO_3 NPs may be used as a solution base for fabrication of hydrogen spray detectors or hydrogen detector tapes (see, for example, https://www.detectape.com/).

Pulsed laser ablation in liquid (PLAL) is a complex process to synthesize NPs in aqueous solutions;[8–13] this approach is based on the reaction between species ejected from the laser exposed target and the solution environment which allows to produce a wide variety of oxides, hydroxides, carbides, sulfides, nitrides, and composite nanostructures[14–18] of the solid target and a small amount of surrounding liquid occurs at the initial periods of the laser-target

Published under license by Laser Institute of America

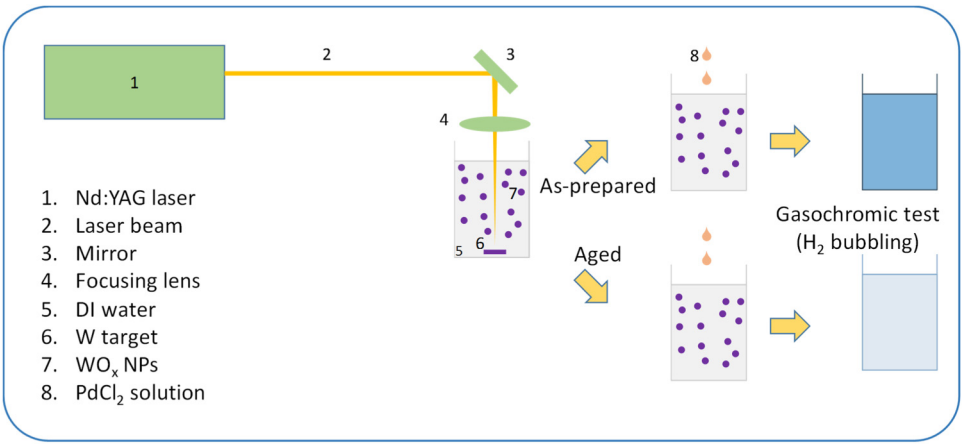

FIG. 1. Schematic representation of PLAL of tungsten target in DI water, adding $PdCl_2$ at different aging times to obtain WO_3-Pd samples and gasochromic coloration of WO_3-Pd colloids after hydrogen bubbling.

interaction. Chemical reactions in the plume generate different species form the target. Because of complicated mechanism behind the PLAL process, many of its details have not been understood yet. Extreme local conditions generated by the pulse of the laser inside the ablation-induced plasma lead to the generation of localized hot place with high pressure resulting in the formation of highly excited dense species in the plume. The interaction between the plasma and the liquid also induces a rapid quenching effect,[19] causing the formation of unusual phases. These unusual phases can be highly reactive so that growth, agglomeration, coagulation, and chemical transformation of different species and particles in the liquid continue for a period of time after the ablation process. Therefore, if a new chemical agent is added to the solution at the initial times of the NP formation, they are expected to reacted, for example, via an oxidation-reduction path, with ablated species and form different biparticles such as core-shells and alloys. On the other hand, an aging period is able to diminish the chemical reactivity of the NPs. Therefore, a study how the aging affects the reactivity of PLAL-derived NPs is of scientific importance.

Accordingly, ablation of W target in water followed by adding a $PdCl_2$ solution is expected to obtain WO_3-Pd core-shell structures, which is able to exhibit the gasochromic hydrogen sensing property. Colloidal WO_3 NPs were previously synthesized by the PLAL method and showed possibility of gasochromic effect with an optimal amount of the added $PdCl_2$.[20] Also, the effect of the preparation conditions such as laser fluence has been studied.[8] From those studies, it could be realized that the aging time before adding $PdCl_2$ after the laser ablation affects the size and morphology of WO_3-Pd NPs, which may also affect their gasochromic response. To our best knowledge, no paper exists on this system which reports the effect of tungsten oxide aging on its reduction ability for palladium chloride conversion. In this paper, the effect of aging of PLAL-derived tungsten oxide colloidal NPs on the ability of palladium to be reduced and its consequences on the gasochromic responses will be examined. The results show that the WO_3-Pd core-shell nanostructures are synthesized in solution only when $PdCl_2$ is added early to the ablation process. The core-shell nanostructures are found to exhibit better gasochromic response probably due to an intimate contact between Pd and WO_3 NPs.

II. MATERIALS AND METHODS

WO_3 NPs were synthesized by the PLAL method in de-ionized (DI) water. The beam of an Nd:YAG laser ($\lambda = 1064$ nm, energy per pulse = 1.2 J, and frequency = 10 Hz) was used. The initial laser beam diameter was 10 mm which was focusing into a 400 μm spot size on the target surface via a 10 cm focal lens and provides a 60 J/cm^2 laser fluence. The beam was delivered for 45 min to a W target (99% purity) placed at the bottom of a vessel containing 250 ml DI water. A $PdCl_2$ solution was prepared by dissolving 0.02 g $PdCl_2$ powder (99.99% purity) in a mixture of 99.9 ml DI water and 0.1 ml HCl. 1 ml of the $PdCl_2$ solution was added to 5 ml of the obtained colloidal WO_3 NPs just after or 0.5, 1, 2, 3, and 24 h after finishing the laser ablation procedure. The samples were named as WP0, WP0.5, WP1, WP2, WP3, and WP24, respectively. The schematic representation of PLAL procedure is plotted in Fig. 1. The crystal structure of the samples was analyzed using an x-ray diffractometer (Philips EXPERT MPD) with Cu-Kα ($\lambda = 1.5418$ Å) radiation. X-ray photoelectron spectroscopy (XPS) analysis was done by an ESCA/AES system. The system is equipped with a concentric hemispherical analyzer (Specs model EA10 plus). For exciting the x-ray photoelectrons, an Al Ka line at 1486.6 eV was used. The energy scale was calibrated according to the carbon binding energy (284.8 eV). Transmission electron microscopy (Philips model CM120) revealed the microstructures of the samples. Specific volumes of colloidal samples were drop-casted on glass substrates for XPS or X-ray diffraction (XRD) analyses. Drop-casted samples of WP24 were also annealed at temperatures of 200 and 500 °C for 2 h in order to study the effect of annealing on the crystal structure. Gasochromic investigations were performed using H_2/Ar mixed gas with different concentrations for coloring of samples and O_2 (purity 99.9%) for their bleaching. The gases were alternatively bubbled into 3 ml of the WO_3-Pd colloidal solutions through a tiny quartz tube. The changes in the color of the solutions during the charging of H_2 gas were measured using a Lambda 950 spectrophotometer (Perkin Elmer). The dynamic responses of the colloidal solutions were investigated by passing a monochromatic light with a wavelength of 630 nm, and the absorption changes were recorded.

Published under license by Laser Institute of America

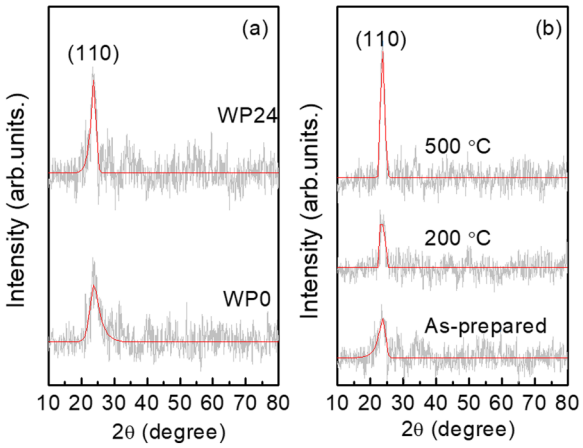

FIG. 2. XRD patterns of (a) samples WP0 and WP24 and (b) sample WP24 after annealing at 200 and 500 °C.

III. RESULTS AND DISCUSSION

A. X-ray diffraction

Figure 2(a) shows the XRD patterns with the fitted asymmetric curves of samples WP0 and WP24. There is only one broad peak at $2\theta = 23.7°$, which is related to the (110) plane of the tetragonal WO_3 structure (JCPS Card No. 85-808). However, the diffraction peak in WP24 is slightly narrower than that of the as-prepared sample indicating, according to Scherrer's relation, that the size of tungsten oxide crystallites has increased over the aging period. No noticeable diffraction peak for palladium is observed probably due to its amorphous nature or low concentration. As it was mentioned above, the laser-target interaction results in a high temperature and pressure cavitation bubble over the target surface during the ablation process that provides favorable thermodynamics conditions for crystallites nucleation. Nevertheless, a postannealing of drop-casted samples of WP24 type at 200 and 500 °C [Fig. 2(b)] has led to an improvement in the crystalline structure. It is worth mentioning that the thermal stability of the tetragonal structure is in high temperatures ranging from 700 to 900 °C.[21]

B. X-ray photoelectron spectroscopy

XPS analysis was used in order to investigate the elemental composition and surface chemical states of the PLAL-derived NPs. The XPS survey scan spectrum of drop-casted sample WP24 is shown in Fig. 3(a). It should be noted that this sample has been actually remained in the lab environment for a long period prior to analyzing. The survey scan spectrum represents the major elemental constituents of O and W in addition to an intense carbon contamination signal at a binding energy of 284.8 eV. In addition, two weak XPS peaks at 99 and 149 eV are originating from the glass substrates. No trace of Pd transitions was detected by XPS due to its very low concentration. Figure 3(b) shows the XPS core level spectrum of W4f which could be deconvoluted into two different doublets. The doublets at the binding energies of 35.6 and 37.8 eV are attributed to W4f7/2 and W4f5/2, respectively. According to the literature, these two peaks are related to the fully oxidized states of tungsten ions (W^{6+}).[22,23] Besides, the doublet including two peaks at 34.4 and 36.4 eV is related to the chemical bonds of W^{5+} oxidation state.[24] The O 1s XPS spectrum has been deconvoluted into two peaks located at 530.8 and 532.7 eV [Fig. 3(c)]. According to the literature, the former peak originates from O–W bonding and the latter is due to the presence of the hydroxyl groups.[25] The higher peak intensity of hydroxyl comparing with W–O suggests that in the laser ablation of tungsten in water, a lot of water molecules are absorbed by the tungsten oxide structure. Using the peak area related to different W4f peaks (W^{6+} and W^{5+}) and that of O1s, the composition of NPs is estimated to be about $WO_{2.8}$. According to XPS results, the presence of W^{5+} states and substoichiometric composition confirms the possibility of the presence of surface oxygen defects even after long aging. These defects are responsible for the high chemical activity of NPs and reduction of $PdCl_2$.

C. Transmission electron microscope (TEM)

Figures 4(a)–4(c) indicate the TEM images and size distribution histograms of samples WP0, WP1, and WP24, respectively.

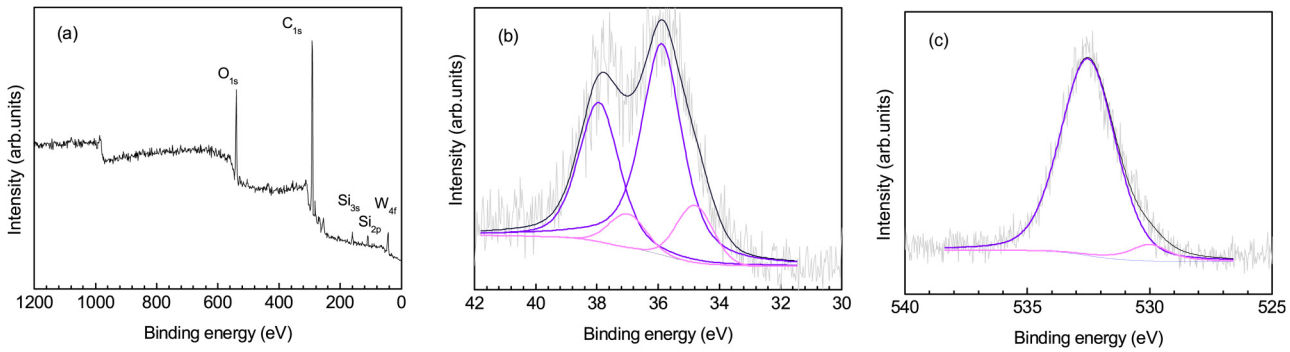

FIG. 3. XPS spectra of sample WP24, (a) survey scan, (b) W4f, and (c) O1s core level transition.

Published under license by Laser Institute of America

The size distribution histogram of sample WP0 reveals that particle size is in the range of 3–25 nm, with about 11 nm average size. In Fig. 4(a), two different types of particles are distinguished according to their gray and black contrasts. With lower atomic number, palladium parts are probably the gray regions and there are several recognizable core-shell particles shown with arrows. The high magnification images inside the figure illustrate the details of WO_3-Pd core-shell structure in which the Pd shell thickness is about 8 nm. This image obviously indicates that several particles are found with a core-shell structure where the thin Pd shell covers completely the surface of the WO_3 NP. This suggests that the combination of the PLAL followed by reduction reaction makes it possible to produce core-shell NPs. The suggested chemical mechanism for Pd^{2+} conversion to metallic Pd is as follows:

$$\begin{gathered} W^{5+}(\text{in the initial } WO_{x(x<3)}) \rightarrow W^{6+}(\text{in } WO_3) + e^-, \\ Pd^{2+} + 2e^- \rightarrow Pd^0(\text{metallic}) \end{gathered} \tag{1}$$

because of the substoichiometric nature of ejected particles, they can be oxidized over aging or by an external agent like Pd^{2+}. When

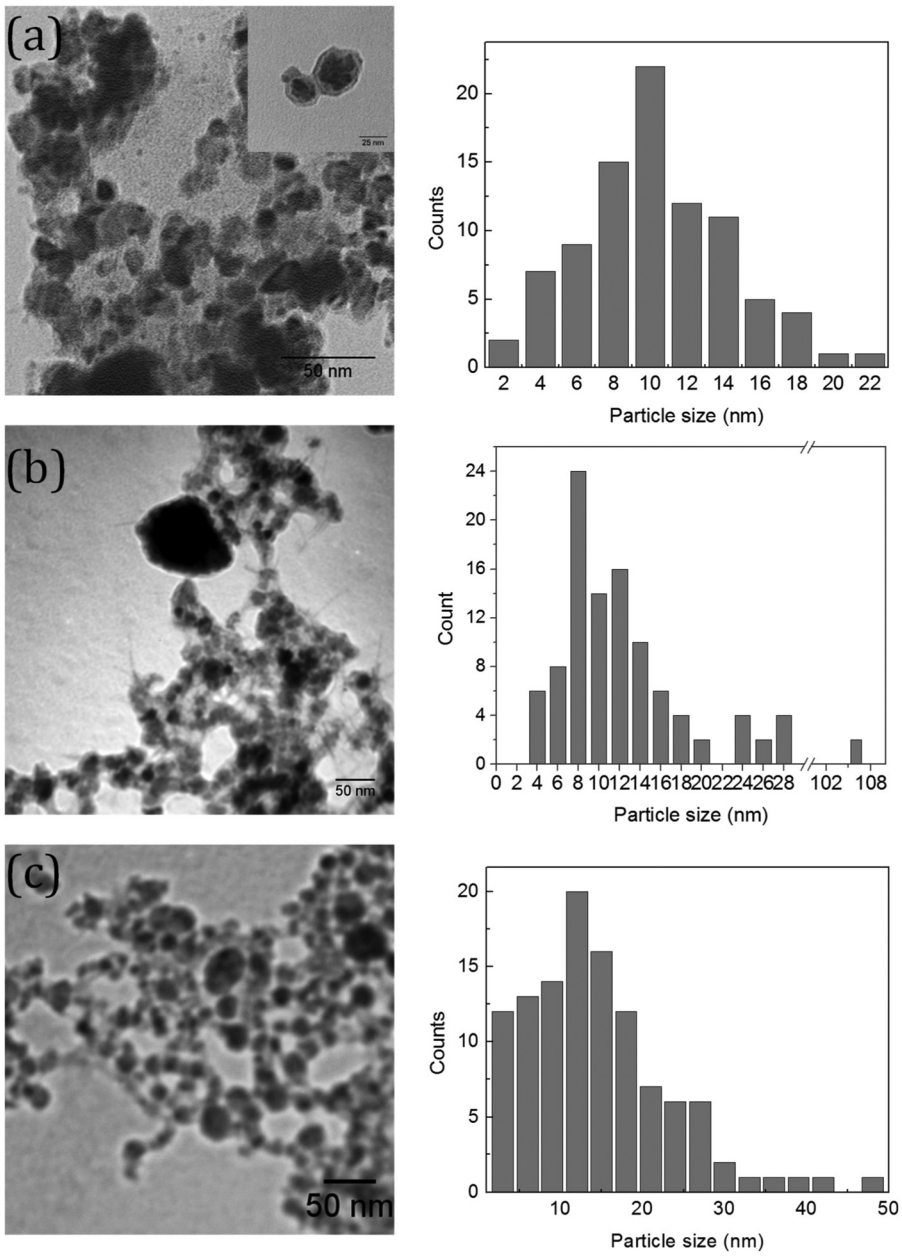

FIG. 4. TEM images and size distribution histograms of sample (a) WP0, (b) WP1, and (c) WP24.

Published under license by Laser Institute of America

$PdCl_2$ is added after 1 h aging in sample WP1, the average particles size increases to ~14 nm [Fig. 4(b)]. Although a few core-shell NPs can be yet observed for sample WP1, TEM micrograph of sample WP24 represents individual particles that are unlikely to have a core-shell structure. Comparing these TEM images clearly shows that the delay time of the $PdCl_2$ solution addition plays a key role in creating a core-shell structure. It seems that the palladium ions are not reduced remarkably at the surface of NPs in sample WP24 in contrast to sample WP0, which is attributed to an aging-induced passivation of the surface chemical reactivity in the WO_3 NPs. Size distribution histogram shown in Fig. 3(b) reveals that the particles size is in the range of 6–52 nm where the average size is determined to be 19 nm. This increase in the average particle size of WO_3 NPs was also confirmed by the XRD (Fig. 2).

D. Optical properties

Figure 5(a) shows the optical transmission spectra of different WO_3-Pd (WP) samples. The spectra show 60%–90% transparency in the visible region with the lowest transparency for sample WP0. The observable small absorption peak at 417 nm (shown by a dashed line) is due to the absorption band of the orangish $PdCl_2$ solution,[26] and the sharp decrease in the transmission at around 300 nm is known to be due to the optical absorption edge.[27] A comparison of the $PdCl_2$ peak for samples WP0 and WP24 is shown in part (b), indicating that this peak strongly reduces in the WP0 sample. It should be noted that reduction of $PdCl_2$ can be understood by variation in its absorption peak.

As is seen, in comparison to the aged samples, this peak has become negligible in sample WP0, indicating decomposition of $PdCl_2$ solution via conversion to metallic palladium structures. The reduced optical transmission can be attributed to the formation of Pd NPs. Tauc plots have been used to determine the overall behavior of optical bandgap, notwithstanding their applicability to conventional 3D bulk material, and they do identify changes in the effective bandgap. The corresponding optical bandgaps are calculated from a linear extrapolation in $(\alpha h\upsilon)^{0.5}$ plot versus photon energy according to the Tauc formulation.[28] The optical bandgaps determined for samples WP0, WP0.5, WP1 WP2, WP3, and WP24 are 3.0, 3.2, 3.2, 3.4, and 3.4 eV

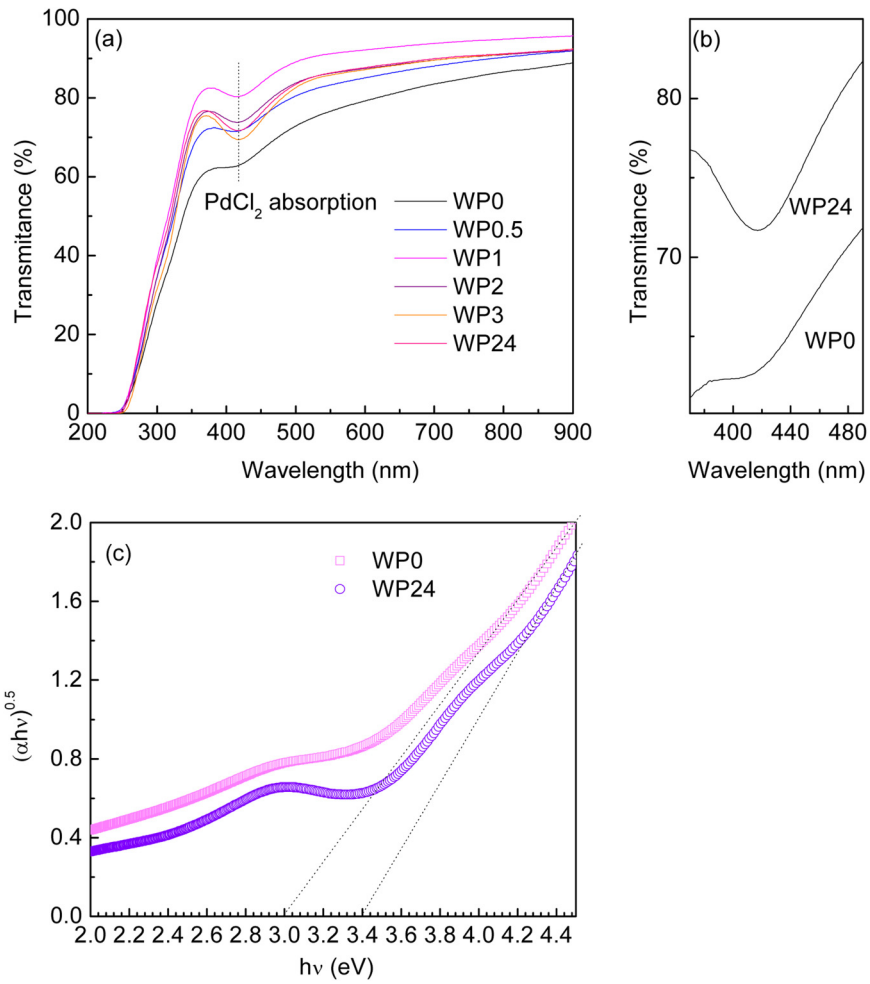

FIG. 5. (a) Optical transmission spectra of WP samples. (b) Details of $PdCl_2$ absorption peak for samples WP0 and WP24 and (c) linear extrapolation for calculation of the optical bandgap of samples WP0 and WP24.

Published under license by Laser Institute of America

respectively [Fig. 5(c)], which are close to those reported for WO_x with different x.[29,30] It should be noted that the bandgap calculation of NPs may deal with an underestimation using the Tauc method because the electronic structure of small particles is wider compared to the bulk. This increase in the optical bandgap was predictable as the oxidation degree of WO_x colloids is expected to increase by spontaneous filling the oxygen vacancies during the aging period. Therefore, the optical observation suggests that the surface chemical reactivity is significant for the mixing process at the early laser ablation times while it is suppressed during the aging period. They also support the speculation about the correlation between surface chemical reactivity and oxidation degree that depends on time. In addition, it perhaps confirms that the core-shell morphology in TEM is a result of decomposing $PdCl_2$ over the very active tungsten oxide surface.

E. Gasochromic hydrogen sensing

When dilute hydrogen gas was bubbled into the colloidal WO_3-Pd solutions, their initial colorless visual reversibly turned an absorbing blue state. Due to the absorbing nature of the gasochromic coloring, we show the absorption spectra instead of their transmittance. Figure 6(a) shows the absorption coefficient difference (ΔA; the magnitude of difference in the absorbance before and after gas exposure) spectra versus the photon energy for different WP samples. Figures 6(b) and 6(c) show typical photographic images of a WO_3-Pd sample before and after hydrogen coloration, respectively. Two absorption bands located at 1.3 and 1.9 eV are clearly seen in all the spectra which are denoted as P_1 and P_2, respectively. These peaks are characteristics for the colored tungsten oxide in the presence of elements such as Li and H.[31] These peaks are attributed to absorption by small polarons or different vibrational modes of localized surface plasmon resonance of defective tungsten oxide.[32,33] The behavior of light absorption by the peak area integral in the range of 1.2–2.5 eV calculated for different samples (not shown here) clearly indicated that the overall absorption decreases with aging and P1 becomes comparable to P2.

To be introduced as gasochromic sensor material, the response features of these colloids should be derived. In the gas sensing evaluations, the hydrogen concentration and the flow rate are the two key parameters. First, the hydrogen concentration effect on the gasochromic switching of the colloidal solutions is studied. To do this, hydrogen and oxygen were bubbled alternatively to the colloidal suspensions of WP0 and WP24 and their optical absorptions were recorded over the time. The H_2 concentrations exposed to the suspensions varied from 10% to 0.5%. The absorption at the constant 630 nm wavelength versus time is shown in Figs. 7(a) and 7(b) for the two different samples. The reversibility of the samples after bubbling of hydrogen and oxygen is clearly observable for both the samples. The response time of the two samples increases by decreasing the H_2 concentration. With an H_2 concentration of 10%, the absorption of WP0 reaches 1.2 after just 5 min, whereas a longer time of more than 40 min is needed for WP24 to reach an absorption of just 0.4. This shows that all response features of the gasochromic effect, including response time and sensitivity, are greater in sample WP0 comparing with sample WP24. The H_2 threshold concentration required to be detected by the colloidal suspensions is very low in the order of 0.5% that is comparable to the WO_3 gasochromic thin films.[34] This suggests that the colloidal solution of WO_3-Pd may be a good candidate to be used as a gasochromic sensing system which addresses the long response time in the gasochromic thin film type sensors.[34,35]

In the following, we study the effect of hydrogen flow rate on the saturated optical absorption at 630 nm constant wavelength by bubbling H_2(10%)/Ar(90%) gas with different flow rates of 2, 5, and 10 Nl/h for 10 min to the different WP samples. The change in the saturated optical absorption, ΔA, is plotted in Fig. 8. It is apparent that ΔA increases with the hydrogen flow rate in all the samples. In the samples with aging time below 3 h, the responses are nearly the same for different flow rates, e.g., they reach an absorption of about 1.1–1.3 in the flow rate of 10 Nl/h. However, in sample WP24, the maximum value of ΔA is

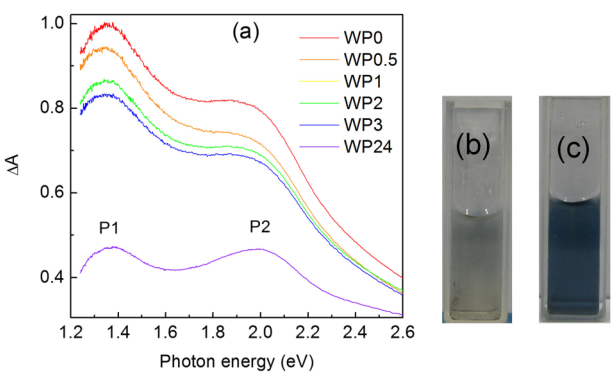

FIG. 6. (a) Optical absorption differences vs photon energy for different WP samples. (b) and (c) represent the photographic images of sample before and after coloration, respectively.

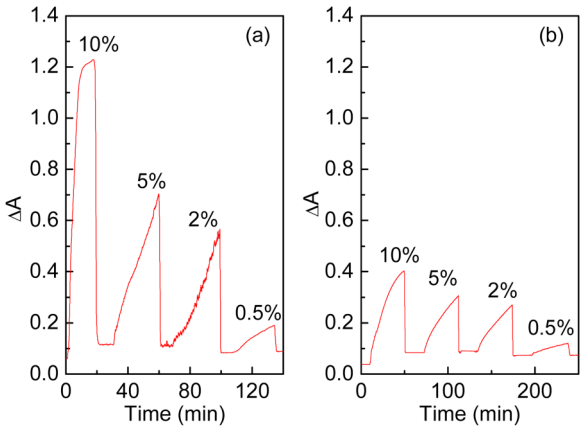

FIG. 7. Absorption differences as a function of hydrogen insertion time for different concentrations at 630 nm constant wavelength: (a) sample WP0 and (b) WP24.

Published under license by Laser Institute of America

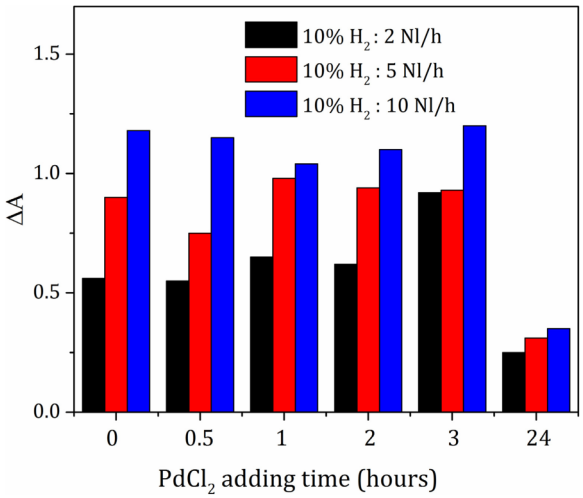

FIG. 8. The changes in absorption of a monochromatic light to the hydrogen gas with different flow rates and the time of adding $PdCl_2$. The H_2 concentration here was constant at 10%.

about 0.4 that is much lower than those with shorter aging time. Here, it is shown that WO_3-Pd core-shell colloidal NPs show better gasochromic responses rather than a liquid containing WO_3 NPs with $PdCl_2$ solution.

F. Mechanism

The mechanism of WO_3-Pd core-shell structure formation is explained in Fig. 9, indicating the schematic representation of NP formation in PLAL and the effect of aging on size and interaction with Pd^{2+} ions. Incidence of the pulsed laser beam to the target surface removes the tungsten species from the target surface, interacts, and nucleates in a cavity region above the target. In the extreme ambient conditions of plume including high temperature, high pressure, and high density of ions, the W species interact strongly together and produce clusters of tungsten components.[36] These clusters begin to interact with the atoms of the solution such as oxygen present in the water and form defective tungsten oxide NPs with active surface which are able to absorb (due to negative surface charges) and convert Pd^{2+} cations. Addition of $PdCl_2$ right after the PLAL process of tungsten target leads to the reduction of Pd^{2+} ions into metallic Pd shell on the surface of $WO_{x(x<3)}$ NPs. The increase in the size of WO_3 NPs upon aging (Fig. 4) indicates that the newly formed NPs probably continue to grow even after finishing the PLAL process. In the absence of palladium ions in a normal aging process, tungsten oxidation continues up to fully WO_3 oxidation for a period of time. Therefore, the growth of the transition metal NPs in water is likely a reactive process and leads to the formation of metal oxide NPs[37,38] that are active at early stages due to surface defects and become passive after aging. The surface defects are not only able to reduce ions, but also act as centers for anchoring supporting NPs. This is why we observed core-shell structures in TEM images.

As it was mentioned, palladium is reduced on and passivates the surface of WO_x NPs via covering and/or oxidizing W^{n+} ions; thus, the WO_3 NPs are seen smaller in the TEM image of sample WP0. Since the gasochromic process is a consequence of hydrogen dissociation on the palladium surface and its penetration into tungsten oxide, it is important to know how palladium and tungsten oxide are in contact and how aging prevents this connection. It can be said that the addition of palladium chloride solution immediately after the laser process results in the formation of the core-shell structure, which also has a better gasochromic response. In a core-shell configuration, the intimate contact between palladium and tungsten oxide results in the direct injection of hydrogen ions (protons) into the tungsten oxide lattice which leads to an increased gasochromic coloration and optical absorption. Moreover, the structure of the palladium shell may be constructed of agglomeration of very small Pd NPs which provides it a porous state and hence facilitates the hydrogen diffusion from the surface to the core. In contrast, in the case of aged WO_3 NP due to insufficient particles connection, little decomposed hydrogens are absorbed inadequately by WO_3 structures leading to a less optical absorption in the gasochromic process.

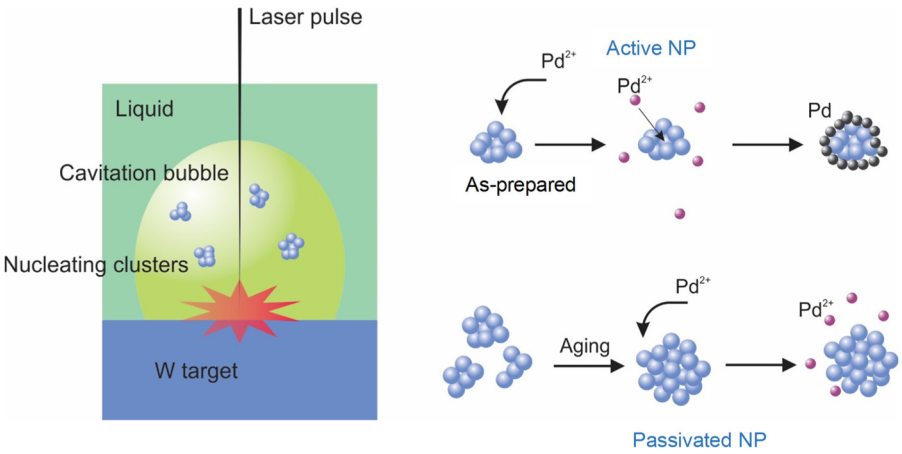

FIG. 9. Schematic representation of laser ablation of W target and the effect of aging on formation the WO_3-Pd core-shell NPs. The aging caused surface passivation of tungsten oxide NPs.

Published under license by Laser Institute of America

IV. CONCLUSIONS

WO_3 NPs were synthesized by PLAL of a W target in DI water. The average diameter of particles experienced an increase of 8 nm by extending the aging time of WO_3 NPs before $PdCl_2$ adding. TEM results revealed the formation of the WO_3-Pd core-shell nanostructures for sample WP0 because of the highly reactivity of the WO_3 cores just after the PLAL process. Pd shell results in a direct injection of decomposed hydrogen atoms from palladium shell to WO_3 pores which leads to an enhancement in the gasochromic response of this sample. The gasochromic response of the WO_3-Pd colloids increases with increasing flow rate and concentration of hydrogen gas. The liquid samples also showed reversible gasochromic response to the different concentrations of H_2 from 0.5% to 10%. It was also proposed that, for experimental condition of this paper, the best time for $PdCl_2$ adding for conditions of this research should not exceed 3 h after the ablation process.

ACKNOWLEDGMENT

The authors would like to thank the Iranian National Science Foundation (INSF) for financial support.

REFERENCES

[1]J. Kukkola, J. Mäklin, N. Halonen, T. Kyllönen, G. Tóth, M. Szabó, A. Shchukarev, J. P. Mikkola, H. Jantunen, and K. Kordás, "Gas sensors based on anodic tungsten oxide," Sens. Actuators B **153**, 293–300 (2011).
[2]J. J. Ho, "Novel nitrogen monoxides (NO) gas sensors integrated with tungsten trioxide (WO_3)/pin structure for room temperature operation," Solid State Electron. **47**, 827–830 (2003).
[3]H. Zheng, J. Z. Ou, M. S. Strano, R. B. Kaner, A. Mitchell, and K. Kalantar-Zadeh, "Nanostructured tungsten oxide - Properties, synthesis, and applications," Adv. Funct. Mater. **21**, 2175–2196 (2011).
[4]V. Wittwer, M. Datz, J. Ell, A. Georg, W. Graf, and G. Walze, "Gasochromic windows," Sol. Energy Mater. Sol. Cells **84**, 305–314 (2004).
[5]M. Ranjbar, N. Tahmasebi Garavand, S. M. Mahdavi, and A. Irajizad, "Electroless plating of palladium on WO_3 films for gasochromic applications," Sol. Energy Mater. Sol. Cells **94**, 201–206 (2010).
[6]W. Feng, G. Wu, and G. Gao, "Ordered mesoporous WO_3 film with outstanding gasochromic properties," J. Mater. Chem. A **2**, 585–590 (2014).
[7]Y. A. Lee, S. S. Kalanur, G. Shim, J. Park, and H. Seo, "Highly sensitive gasochromic H_2 sensing by nano-columnar WO_3-Pd films with surface moisture," Sens. Actuators, B **238**, 111–119 (2017).
[8]N. T. Garavand, S. M. Mahdavi, and A. Iraji Zad, "Pd^{2+} reduction and gasochromic properties of colloidal tungsten oxide nanoparticles synthesized by pulsed laser ablation," Appl. Phys. A Mater. Sci. Process. **108**, 401–407 (2012).
[9]R. M. Tilaki, A. Irajizad, and S. M. Mahdavi, "Stability, size and optical properties of silver nanoparticles prepared by laser ablation in different carrier media," Appl. Phys. A Mater. Sci. Process. **84**, 215–219 (2016).
[10]A. Georg, W. Graf, R. Neumann, and V. Wittwer, "Mechanism of the gasochromic coloration of porous WO_3 films," Solid State Ionics **127**, 319–328 (2000).
[11]Y. Li, O. R. Musaev, J. M. Wrobel, and M. B. Kruger, "Laser ablation in liquids of germanium in externally applied electric fields," J. Laser Appl. **28**, 022004 (2016).
[12]S. Li, Y. Zhao, Y. Jiang, and Y. Zhang, "Preparation and properties of noble metal core/shell nanostructures prepared by excimer laser ablation in liquid solutions," J. Laser Appl. **26**, 022001 (2014).
[13]P. Nachev, D. D. van 'T Zand, V. Coger, P. Wagener, K. Reimers, P. M. Vogt, S. Barcikowski, and A. Pich, "Synthesis of hybrid microgels by coupling of laser ablation and polymerization in aqueous medium," J. Laser Appl. **24**, 042012 (2012).
[14]S. C. Singh and R. Gopal, "Laser irradiance and wavelength-dependent compositional evolution of inorganic ZnO and ZnOOH/organic SDS nanocomposite material," J. Phys. Chem. C **112**, 2812–2819 (2008).
[15]N. Takada, T. Sasaki, and K. Sasaki, "Synthesis of crystalline TiN and Si particles by laser ablation in liquid nitrogen," Appl. Phys. A Mater. Sci. Process. **93**, 833–836 (2008).
[16]K. V. Anikin, N. N. Melnik, A. V. Simakin, G. A. Shafeev, V. V. Voronov, and A. G. Vitukhnovsky, "Formation of ZnSe and CdS quantum dots via laser ablation in liquids," Chem. Phys. Lett. **366**, 357–360 (2002).
[17]C. N. Huang, J. S. Bow, Y. Zheng, S. Y. Chen, N. J. Ho, and P. Shen, "Nonstoichiometric titanium oxides via pulsed laser ablation in water," Nanoscale Res. Lett. **5**, 972–985 (2010).
[18]A. Menéndez-Manjón, A. Schwenke, T. Steinke, M. Meyer, U. Giese, P. Wagener, and S. Barcikowski, "Ligand-free gold-silver nanoparticle alloy polymer composites generated by picosecond laser ablation in liquid monomer," Appl. Phys. A Mater. Sci. Process. **110**, 343–350 (2013).
[19]H. Zeng, C. Zhi, Z. Zhang, X. Wei, X. Wang, W. Guo, Y. Bando, and D. Golberg, "'White graphenes': Boron nitride nanoribbons via boron nitride nanotube unwrapping," Nano Lett. **10**, 5049–5055 (2010).
[20]M. Ranjbar, H. Kalhori, S. M. Mahdavi, and A. I. Zad, "New gasochromic system: Nanoparticles in liquid," J. Nanoparticle Res. **14**, 803 (2012).
[21]A. Garg, J. A. Leake, and Z. H. Barber, "Epitaxial growth of WO_3 films on $SrTiO_3$ and sapphire," J. Phys. D: Appl. Phys. **33**, 1048–1053 (2000).
[22]F. Di Gregorio and V. Keller, "Activation and isomerization of hydrocarbons over WO_3/ZrO_2 catalysts: I. Preparation, characterization, and X-ray photoelectron spectroscopy studies," J. Catal. **225**, 45–55 (2004).
[23]T. H. Fleisch and G. J. Mains, "An XPS study of the UV reduction and photochromism of MoO_3 and WO_3," J. Chem. Phys. **76**, 780–786 (1982).
[24]R. J. Colton, A. M. Guzman, and J. W. Rabalais, "Electrochromism in some thin-film transition-metal oxides characterized by x-ray electron spectroscopy," J. Appl. Phys. **49**, 409–416 (1978).
[25]R. R. Kharade, S. S. Mali, S. P. Patil, K. R. Patil, M. G. Gang, P. S. Patil, J. H. Kim, and P. N. Bhosale, "Enhanced electrochromic coloration in Ag nanoparticle decorated WO_3 thin films," Electrochim. Acta **102**, 358–368 (2013).
[26]S. A. Chimatadar, S. B. Koujalagi, and S. T. Nandibewoor, "Oxidation of palladium(II) by hexacyanoferrate(III) in aqueous ethanoic acid: A mechanistic study," Transit. Met. Chem. **27**, 62–68 (2002).
[27]T. He, Y. Ma, Y. Cao, X. Hu, H. Liu, G. Zhang, W. Yang, and J. Yao, "Photochromism of WO_3 colloids combined with TiO_2 nanoparticles," J. Phys. Chem. B **106**, 12670–12676 (2002).
[28]J. Tauc, R. Grigorovici, and A. Vancu, "Optical properties and electronic structure of amorphous germanium," Phys. Status Solidi **15**, 627–637 (1966).
[29]P. P. González-Borrero, F. Sato, A. N. Medina, M. L. Baesso, A. C. Bento, G. Baldissera, C. Persson, G. A. Niklasson, C. G. Granqvist, and A. Ferreira Da Silva, "Optical band-gap determination of nanostructured WO_3 film," Appl. Phys. Lett. **96**, 061909 (2010).
[30]S. Adhikari and D. Sarkar, "Hydrothermal synthesis and electrochromism of WO_3 nanocuboids," RSC Adv. **4**, 20145–20153 (2014).
[31]M. Ranjbar, A. Heidari Fini, H. Kalhori, P. Kameli, and H. Salamati, "Gasochromic effect in colloidal nanoparticles of tungsten oxide dihydrate synthesized via a simple anodizing method," Sol. Energy Mater. Sol. Cells **132**, 329–336 (2015).
[32]O. F. Schirmer and E. Salje, "The W^{5+} polaron in crystalline low temperature WO_3 ESR and optical absorption," Solid State Commun. **33**, 333–336 (1980).
[33]K. Manthiram and A. P. Alivisatos, "Tunable localized surface plasmon resonances in tungsten oxide nanocrystals," J. Am. Chem. Soc. **134**, 3995–3998 (2012).
[34]C. H. Hsu, C. C. Chang, C. M. Tseng, C. C. Chan, W. H. Chao, Y. R. Wu, M. H. Wen, Y. T. Hsieh, Y. C. Wang, C. L. Chen *et al.*, "An ultra-fast response gasochromic device for hydrogen gas detection," Sens. Actuators, B **186**, 193–198 (2013).

Published under license by Laser Institute of America

[35]D. Li, G. Wu, G. Gao, J. Shen, and F. Huang, "Ultrafast coloring-bleaching performance of nanoporous WO_3-SiO_2 gasochromic films doped with Pd catalyst," ACS Appl. Mater. Interfaces **3**, 4573–4579 (2011).
[36]T. Sasaki, Y. Shimizu, and N. Koshizaki, "Preparation of metal oxide-based nanomaterials using nanosecond pulsed laser ablation in liquids," J. Photochem. Photobiol. A **182**, 335–341 (2006).
[37]R. Prakash, D. M. Phase, R. J. Choudhary, and R. Kumar, "Structural, electrical, and magnetic properties of $Mo_{1-x}Fe_xO_2$ ($x = 0$–E0.05) thin films grown by pulsed laser ablation," J. Appl. Phys. **103**, 043712 (2008).
[38]M. Ranjbar, S. M. Mahdavi, and A. Iraji zad, "Pulsed laser deposition of W-V-O composite films: Preparation, characterization and gasochromic studies," Sol. Energy Mater. Sol. Cells **92**, 878–883 (2008).

Published under license by Laser Institute of America